MODIFIED PARALLEL-STRUCTURED SIGNAL DECOMPOSITION ALGORITHM FOR ENHANCED POWER QUALITY AND DEMAND SIDE RESPONSE IN STANDALONE DISTRIBUTED GENERATION

Lingappa Jaklair[1*]– Guduri Yesuratnam[1] – Pannala Mallikarjuna Sarma[2]

[1]Electrical Engineering Department, University College of Engineering, Hyderabad, Telangana, India
[2]Electrical Engineering Department, Vasavi College of Engineering, Hyderabad, Telangana, India

ARTICLE INFO

***Article history*:**
Received: 08.04.2024.
Received in revised form: 15.03.2025.
Accepted: 25.03.2025.

Keywords:
Frequency-locked loop (FLL)
Parallel signal decomposition
Demand side response
Three-phase systems
Load unbalance

DOI: https://doi.org/10.30765/er.2494

Abstract:

This paper presents the comprehensive solution of demand side response and enhanced power quality in a standalone distributed generation system using modified parallel structured signal decomposition control algorithm (MPSSD). It is observed that in most of the conventional frequency locked loop (FLL) based algorithm dual-reduced order generalized integrator-frequency locked loop (DROGI-FLL), the estimation of fundamental frequency positive and negative sequence components of load current in the αβ frame is primarily required to generate the source reference current for solving the power quality and demand response issues. However, modified parallel structured signal decomposition control algorithm (MPSSD) estimates the said both components directly without involvement of αβ frame transformation. Therefore, computational burden and estimation time requirement is reduced. As a result, the faster and high accurate dynamic response of proposed MPSSD control algorithm is achieved under transient behavior of distributed generation system. The main objectives in this paper is to provide harmonics free source current, load balancing under different demand side response conditions and reactive power control in solar-wind based distributed power generation system. This task is achieved by operating the voltage source converter through the switching patterns generated by MPSSD control algorithm. The entire system is built in MATLAB Simulink and results of various operating conditions are observed and found satisfactory.

1 Introduction

In the 21st century, environmental pollution has evolved into a major global issue, leading to numerous life-threatening incidents over the past two decades [1]. The primary contributors to this issue are conventional power generation methods, industrial captive power plants, and public or private transportation vehicles [2]. Consequently, the shift towards renewable energy generation and efficient power management is crucial for modern society. Harnessing renewable sources like solar, wind, biomass, and tidal energy at the receiving end, particularly at low voltage levels, can help mitigate these challenges. Additionally, there is an urgent need for research and development to modernize the conventional power generation systems [3]. Historically, the customer side of the power system has been passive, but this trend must change in the face of evolving energy demands [4].]. However, with

* Corresponding author
E-mail address:lingappa.ou@gmail.com

substantial research on renewable power generation and its integration into the main grid, local power generation and distribution have become almost indispensable.

This approach offers several advantages: first, customers become more aware of their energy generation and can meet their own demand independently; second, they actively support utilities, providing time for modernization. The key challenge lies in the operation and control of renewable energy sources, particularly solar and wind, at the receiving end. This paper focuses on the operational challenges and power management strategies for integrating renewable energy at the low-voltage distribution level. A major concern is synchronizing solar and wind energy, and the control algorithm discussed in [5], which extracts positive, negative, and zero sequence components of voltage and current, offers a solution but is limited to three-phase, four-wire systems. Its effectiveness under varying voltage and current magnitudes is untested, making the Amplitude Adaptive Notch Filter from [6] a potentially better option, as it adapts to frequency variations. Distributed power generation from the customer side introduces low inertia, making frequency and voltage sensitive to load changes. The control algorithm from [7], which features inner current control loops, is well-suited to address this. A discussion on frequency stability in photovoltaic microgrids is presented in [8], emphasizing the crucial role of frequency and phase estimation in synchronization. Various techniques for phase-locked loops (PLLs) are explored in [9], including voltage controlled oscillator (VCO)-less PLL and Cascaded Time Delay Phase Locked Loop (PLL). Another grid synchronization control algorithm, complex coefficient-reduced order generalized integrator (CC-ROGI) FLL, is introduced in [10].

Various power quality issues are addressed using the same control algorithm. The authors in [11] present the application of delayed-PLL for synchronizing solar-wind hybrid power generation, solving objectives like voltage, frequency, and phase estimation, which are crucial for generating reference current and extracting fundamental components for power converters. In [12], PLL with complex gains is discussed, while [13] elaborates on using VCO-less PLL to address power quality issues in wind energy systems. Other simpler PLL-based techniques are outlined in [14].Frequency adaptiveness problems are addressed in [15], where earlier voltage phase angle estimation relied on scalar concepts. A vector-based approach for three-phase grid voltage estimation is explored in [16]. Lorentzian filters for resolving power quality issues are discussed in [17]. Additionally, mathematical transforms like fast fourier transform (FFT), Wavelet, and Hilbert for feature extraction are explained in [18-20]. Delayed signal cancellation is another key technique, useful for separating real current components, as seen in [21-23]. Initially applied in electrical drives [24], this method is also applied in distributed power generation systems for terminal and DC link voltage control [25].However, most PLL-based or delayed signal cancellation algorithms are less effective during severe grid disturbances. A combination of frequency-adaptive and delayed signal cancellation algorithms is suggested in [26], with similar signal decomposition techniques reported in [27], highlighting their stability benefits. Yet, their application to distributed power generation systems for addressing power demand response and power quality remains unexplored [28].Therefore, authors have decided it to implement in the proposed system here.

The contribution of the author given below is in this paper:

- Modified Parallel-Structured Signal Decomposition Algorithm is proposed for the evaluation of phase angle, frequency, and the active fundamental component of load current of the proposed system.
- Voltage source converter (VSC) with Modified Parallel-Structured Signal Decomposition Algorithm enhances the power quality of wind-driven three-phase self-excited induction generator (SEIG) in isolated applications under fixed/varying insolation, fixed/varying wind speed and linear/nonlinear load.
- The utilization of maximum power point tracking (MPPT) approach employing incremental conductance (IC) method aims to adjust the duty cycle dynamically to optimize solar power extraction across varying insolation levels.

- BESS coupled with VSC offers active/reactive power assistance at point of common coupling (PCC).

2 Proposed Configuration of the System

Figure.1 depicts system configuration is taken for the assessment of practical feasibility in standalone mode of 3P3W wind-solar distributed power generation system under various operating conditions. This setup comprises a wind turbine serving as the primary driver for the SEIG. The capacitor bank is used for self-excited SEIG and generates nominal voltage at no load condition.

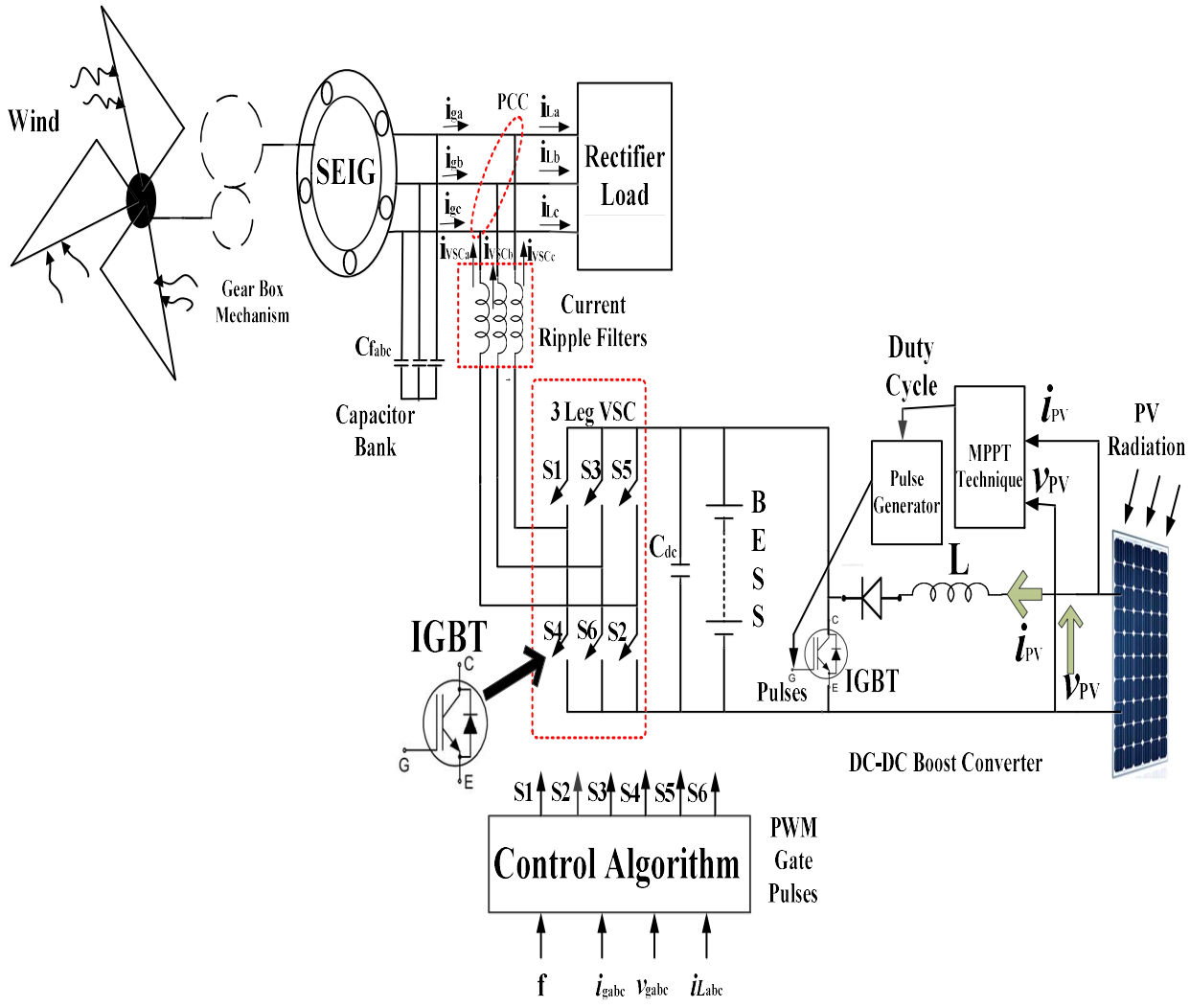

Figure.1 Block Diagram of Proposed System

Moreover, employing the MPPT technique utilizing the incremental conductance (IC) method optimizes power extraction from the PV array across changing irradiation levels. A current-controlled voltage source converter (CC-VSC) is built using six insulated gate bipolar transistors (IGBT) legs, with interfacing inductors facilitating connection between the VSC and SEIG. A balanced load, either linear or nonlinear, is linked at the consumer end, while a battery energy storage system (BESS) is connected at the DC terminal of the VSC. The BESS compensates for power deficits during reduced wind speeds or high load demands by discharging the battery. Conversely, during high wind speeds or low load demands, the BESS assists in managing surplus power.

3 Modified Parallel-Structured Signal Decomposition Algorithm(MPSSD) for VSC

3.1 Reference Current Extraction

The modern power converter (voltage source converters) is widely used in such type of renewable system where power quality and demand side management is required. To address the above issues, signal processing control algorithms are often involved for fundamental load current extraction and estimation. The discrete-fourier transform (DFT) is usual choice due to its faster computational speed. However, it is always a reluctant solution in case of selective frequency component extraction. In such circumstances, time-domain signal decomposition algorithms are often preferred. Additionally, these control algorithms represent nonlinear feedback systems comprising two or more dynamically interactive frequency-adaptive filters, precisely tuned to the relevant frequency components the selected Modified Parallel-Structured Signal Decomposition Algorithm lie in the similar domain and provided in Figure.2 and Figure.3.

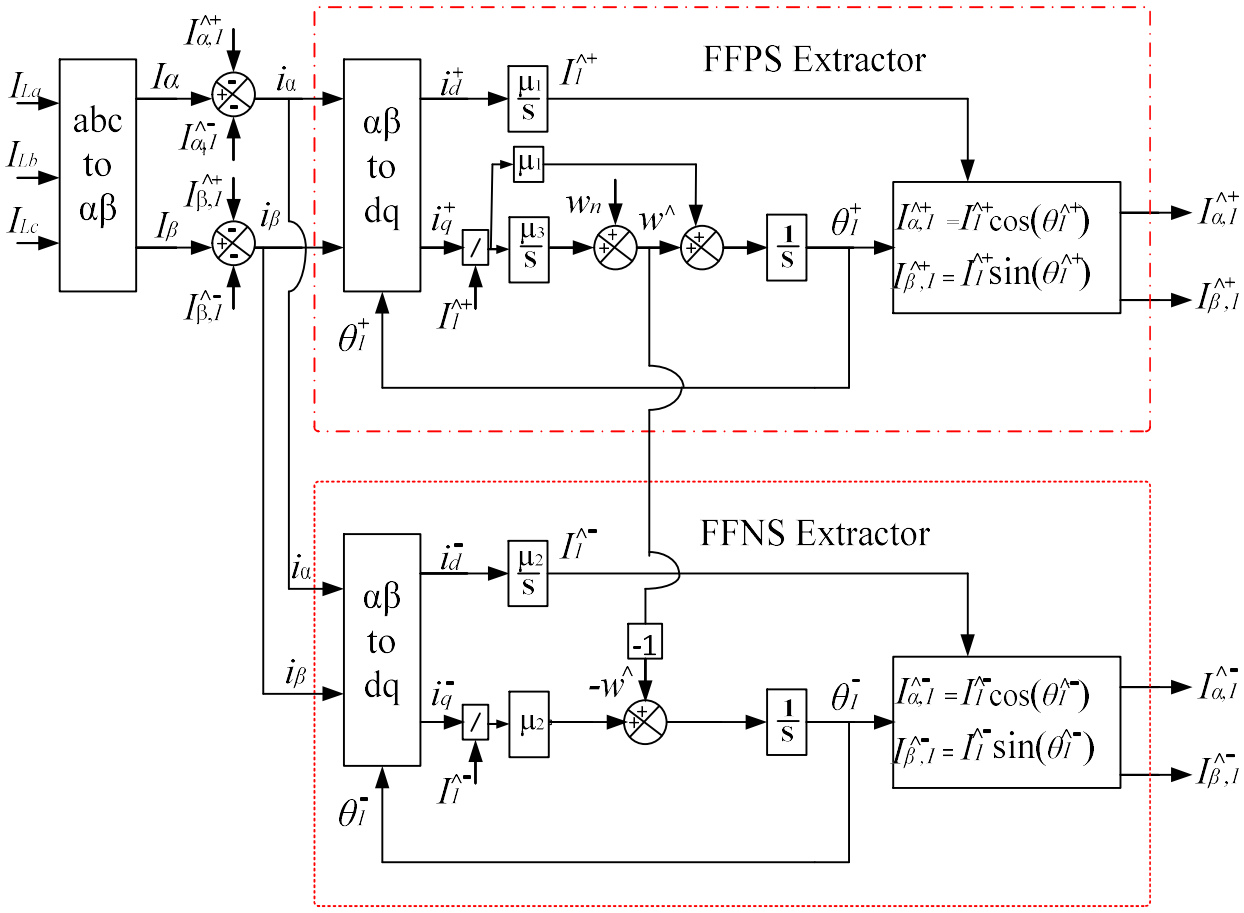

Figure.2 Block diagram of MPSSD. μ_1, μ_2, and μ_3 are the control parameters. $I_{\alpha,1}^{\Lambda+}$ and $I_{\beta,1}^{\Lambda+}$ are estimations of the fundamental frequency positive sequence(FFPS) component of the load current in the αβ frame. $\theta_1^{\Lambda+}$ and $I_1^{\Lambda+}$ are the estimation of the phase angle and amplitude of the FFPS component of the load current. w^{Λ} is an estimation of angular frequency of the load current. $I_{\alpha.1}^{\Lambda-}$ and $I_{\beta.1}^{\Lambda-}$ are estimations of the fundamental frequency negative sequence(FFNS) component of the load current in the αβ frame. $\theta_1^{\Lambda-}$ and $I_1^{\Lambda-}$ are the estimation of the phase angle and amplitude of the FFNS component of the load current.

W_n =2π50 rad/s.

It seems that the structures of these algorithms are easy to implement for power quality improvement and demand side management in the proposed system. The detail description of this algorithm for feature selection is given here below:

$$\begin{bmatrix} i_d^+ \\ i_q^+ \end{bmatrix} = \begin{bmatrix} \cos(\hat{\theta}_1^+) & \sin(\hat{\theta}_1^+) \\ -\sin(\hat{\theta}_1^+) & \cos(\hat{\theta}_1^+) \end{bmatrix} \begin{bmatrix} i_\alpha \\ i_\beta \end{bmatrix} \quad (1)$$

$$= \frac{1}{\hat{\imath}_1^+} \begin{bmatrix} \hat{\imath}_{\alpha,1}^+ & \hat{\imath}_{\beta,1}^+ \\ -\hat{\imath}_{\beta,1}^+ & \hat{\imath}_{\alpha,1}^+ \end{bmatrix} \begin{bmatrix} i_\alpha \\ i_\beta \end{bmatrix} \quad (2)$$

$$\begin{bmatrix} i_d^- \\ i_q^- \end{bmatrix} = \begin{bmatrix} \cos(\hat{\theta}_1^-) & \sin(\hat{\theta}_1^-) \\ -\sin(\hat{\theta}_1^-) & \cos(\hat{\theta}_1^-) \end{bmatrix} \begin{bmatrix} i_\alpha \\ i_\beta \end{bmatrix} \quad (3)$$

$$= \frac{1}{\hat{\imath}_1^-} \begin{bmatrix} \hat{\imath}_{\alpha,1}^- & \hat{\imath}_{\beta,1}^- \\ -\hat{\imath}_{\beta,1}^- & i_{\alpha,1}^- \end{bmatrix} \begin{bmatrix} i_\alpha \\ i_\beta \end{bmatrix} \quad (4)$$

Where, $i_\alpha = i_\alpha - i_{\alpha,1}^- - \hat{\imath}_{\alpha,1}^-$, and $i_\beta = i_\beta - \hat{\imath}_{\beta,1}^- - \hat{\imath}_{\beta,1}^-$

$$\frac{d\hat{\imath}_1^+}{dt} = \mu_1 i_d^+ = \frac{\mu_1}{\hat{\imath}_1^+}\left[\hat{\imath}_{\alpha,1}^+ i_\alpha + i_{\beta,1}^+ i_\beta\right] \quad (5)$$

$$\frac{d\hat{\theta}_1^+}{dt} = \hat{\omega} + \frac{\mu_1}{\hat{V}_1^+} e_q^+ = \hat{\omega}\frac{\mu_1}{(\hat{V}_1^+)^2}\left[-\hat{\imath}_{\beta,1}^+ i_\alpha + \hat{\imath}_{\alpha,1}^+ i_\beta\right] \quad (6)$$

$$\frac{d\hat{\imath}_1^-}{dt} = \mu_2 i_d^- = \frac{\mu_2}{\hat{V}_1^-}\left[\hat{\imath}_{\alpha,1}^- i_\alpha + \hat{\imath}_{\beta,1}^- i_\beta\right] \quad (7)$$

$$\frac{d\hat{\theta}_1^-}{dt} = -\hat{\omega} + \frac{\mu_2}{\hat{\imath}_1^-} i_q^- = -\hat{\omega}\frac{\mu_2}{(\hat{\imath}_1^-)^2}\left[-\hat{\imath}_{\beta,1}^- e_\alpha + \hat{\imath}_{\alpha,1}^- i_\beta\right] \quad (8)$$

$$\frac{d\hat{\omega}}{dt} = \frac{\mu_3}{(\hat{\imath}_1^+)^2} i_q^+ = \frac{\mu_3}{(\hat{\imath}_1^+)^2}\left[-i_{\beta,1}^+ i_\alpha + i_{\alpha,1}^+ i_\beta\right] \quad (9)$$

The above equations are harmonic modeling equation that governs entire extraction procedure. The equations provide insight into identifying the fundamental positive and negative sequence components. The various gain parameters are tuned in such a manner that eliminates the multiple frequency components from the load current and only provides the fundamental orthogonal current vector that can be used for reference current generator for voltage source converter. The methods for reference current generation have been discussed further in the following subsections

3.2 Estimation of voltage amplitude and unit voltage template generation

At point of common coupling, the line voltages (v_{ab}, v_{bc}, v_{ca}) are sensed by ac voltage sensor circuit and these are converted into phase voltage (v_{pa}, v_{pb}, v_{pc}) for further processing. The process of conversion is given here as below in equations (10-12):

$$v_{pa} = \frac{1}{3}(2v_{ab} + v_{bc}) \quad (10)$$

$$v_{pb} = \frac{1}{3}(-v_{ab} + v_{bc}) \quad (11)$$

$$v_{pc} = \frac{1}{3}(-v_{ab} - 2v_{bc}) \quad (12)$$

The magnitude of peak terminal voltage (Vm) at PCC can be evaluated can be evaluated as in equation (13):

$$V_m = [0.66(v_{pa}^2 + v_{pb}^2 + v_{pc}^2)]^{\frac{1}{2}} \quad (13)$$

Where, the estimated phase voltages $v_{pa}, v_{pb} and v_{pc}$ are 3-ph instantaneous values. The in phase unit

voltage template can be assessed with the help of instantaneous voltages divided by the voltage amplitude (V_m).

$$p_{ua} = {}^{v_{pa}}/_{V_m}, p_{ub} = {}^{v_{pb}}/_{V_m}, p_{uc} = {}^{v_{pc}}/_{V_m} \tag{14}$$

The quadrature phase unit voltage vectors can be evaluated using the in-phase unit voltage template and conversion matrix as given below in equation (15):

$$\begin{pmatrix} q_{ua} \\ q_{ub} \\ q_{uc} \end{pmatrix} = \frac{1}{\sqrt{3}} \begin{pmatrix} -1 & 0 & 1 \\ \sqrt{3} & 1 & -1 \\ -\frac{\sqrt{3}}{2} & \frac{1}{2} & -\frac{1}{2} \end{pmatrix} \begin{pmatrix} p_{ua} \\ p_{ub} \\ p_{uc} \end{pmatrix} \tag{15}$$

Where, $(p_{ua}, p_{ub}, p_{uc})$are the in phase unit voltage template while $(q_{ua}, q_{ub}, q_{uc})$are the template for quadrature phase unit voltage.

3.3 Generation of Switching Pulses for three leg Voltage Source Converter

After the extraction of fundamental component of load current (I_m) in Figure.2, the process starts for switching pulses generation. To determine the instantaneous value, the fundamental component of the load current (I_m) is multiplied by a fundamental quadrature component. In this evaluation process, the active and reactive component of reference current is obtained via two separate estimation path. In the first estimation path, in phase unit voltage template is fed to zero crossing detector (ZCD) circuit for sensing the zero crossings of said template followed by super imposition of instantaneous value of the fundamental component of load current component and output of ZCD at Sample and Hold(S/H) circuit. The net fundamental active component of load current in the form of dc value is obtained through this process. In order to obtain smooth dc value, low pass filter is also used with cut off frequency of 8 rad/sec. The output of low pass filter (LPF) is active component (i_{Lfr}) of fundamental load current and is added to the photovoltaic (PV) current (i_{pv}) and subtracted with the output of the PI controller (i_{fd}) to obtain the total of active component of reference source current. The current component (i_{fd}) is obtained from the frequency error processed in PI Controller kept in outer frequency correction loop. For better understanding of the readers, the complete process is depicted in Figure.3 with the help of block diagram. From the value of reference frequency (*f**) which is generally kept 50 Hz and actual sensed frequency (*f*), the output of the PI controller would be evaluated as follows.

The differential frequency at the z^{th} sampling instant is obtained as follows:

$$f(z) = f^*(z) - f(z) \tag{16}$$

Where the power loss is represented by i_{fp} (z), the gain constants for the PI controller are denoted as $k_d$and k_i. The active component of the reference source current is computed as follows:

$$i_{Lp} = i_{fp} + i_{pv} - i_{Lfr} \tag{17}$$

$$i_{Lp}^* = i_{Lp}(p_{ua}, p_{ub}, p_{uc}) \tag{18}$$

The reference current (i_{Lq}) is determined by calculating the difference between the reactive component (i_{Lfq}) of the fundamental load current and the output current (i_{smq}). The calculation of the current component (i_{smq}) can be derived as follows.

The voltage error (v_{terr}) for a PCC voltage at z[th] sampling instant is evaluated as

$$v_{merr}(z) = v_m^*(z) - v_m(z) \tag{19}$$

The magnitude of the reference source current (i_{Lq}), which represents the reactive component, is determined by subtracting the reactive component of the fundamental load current i_{Lfq} from the output current i_{smq} .This calculation is expressed as follows :

$$i_{Lq} = i_{smq} - i_{Lfq} \tag{20}$$

$$i_{Lq}^* = i_{Lq}(q_{ua}, q_{ub}, q_{uc}) \tag{21}$$

The following relationship calculates the reference source currents

$$i_{gabc}^* = i_{Lp}^* + i_{Lq}^* \tag{22}$$

For the generation of gate pulses, the sensed source currents (i_{gabc}) and extracted (i_{gabc}^*) are fed to the pulse-width modulation input [19].

3.4 Design of PV system & MPPT Algorithm

The PV system utilizes the Incremental Conductance (IC) MPPT method to optimize power extraction from a solar PV array by adjusting the duty cycle accordingly. At the maximum power point, the derivative of power with respect to voltage ($dp/dv = 0$) equals zero. The IC process is mathematically described as follows:

$$\frac{di_{pv}}{dv_{pv}} > -\frac{i_{pv}}{v_{pv}} \text{then } d_{new} = d_{old} + \Delta d \tag{23}$$

$$\frac{di_{pv}}{dv_{pv}} = -\frac{i_{pv}}{v_{pv}} \text{then } d_{new} = d_{old} \tag{24}$$

$$\frac{di_{pv}}{dv_{pv}} < -\frac{i_{pv}}{v_{pv}} \text{ then } d_{new} = d_{old} - \Delta d \tag{25}$$

$d_{old}, and\ \Delta d$ are the estimated, old and change in duty ratio. The estimated, previous and change in duty ratio are $d_{new,} d_{old}, and\ \Delta d$ essential parameters in the MPPT process. Through an Incremental Conductance(IC) algorithm, the MPPT is continuously adjusted to track the optimal point. The primary goal of MPPT is to regulate the boost converter's duty ratio to maximize power extraction power from the PV array. To enhance performance an integral controller and proportional integral are employed to minimize steady-state error and signal fluctuations.[20].

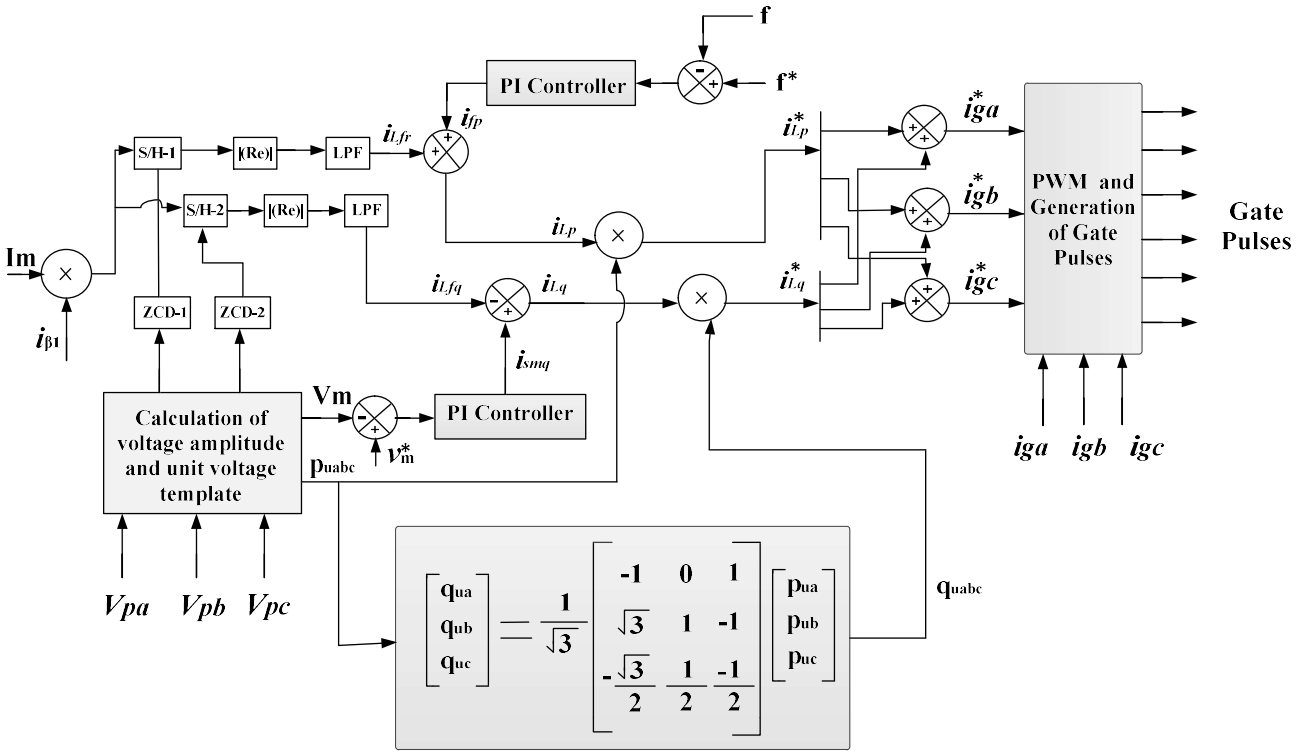

Figure.3 Block diagram of Reference Current Generation for Voltage Source Converter

4 Simulation Performance

The entire system undertaken for this study is developed in MATLAB Simulink and detail simulations are performed under various operating conditions of input and output. The results obtained are arranged and discussed in subsequent subsections provided here below.

4.1 Performance under unbalanced loading and variable wind speed conditions

This operation is carried out when nonlinear load was connected at PCC. The main aim of this work is to assess the efficacy of the employed control algorithm in regulating the source voltage (V_{gabc}) and frequency (f) at the PCC. Additionally, the study focused on mitigating harmonics in the source current (i_{gabc}) and managing power demand on the load side amidst dynamic changes.The above objectives are observed in Figure.4

When the load of phase ‘a’ is removed at t = 1.9 s to 2 s, the battery starts charging and extra power is drawing by BESS. The proposed controller controls the frequency and voltage profile, current profile, and dc link voltage during the variation of load. The source current is maintained balanced even under unbalanced load conditions.

When the wind speed(Ws) is suddenly decreased from 17m/s to 14m/s at t = 2.0 s. Resultantly wind power generation is decreased and deficit load power, which are amplified by the BESS through VSC.Therefore, compensator current is slightly increased, and battery charging current is reduced after t = 2.0 s. During decrease in wind speed, BESS switches from charging to discharging mode and maintains the balance of power at (PCC).

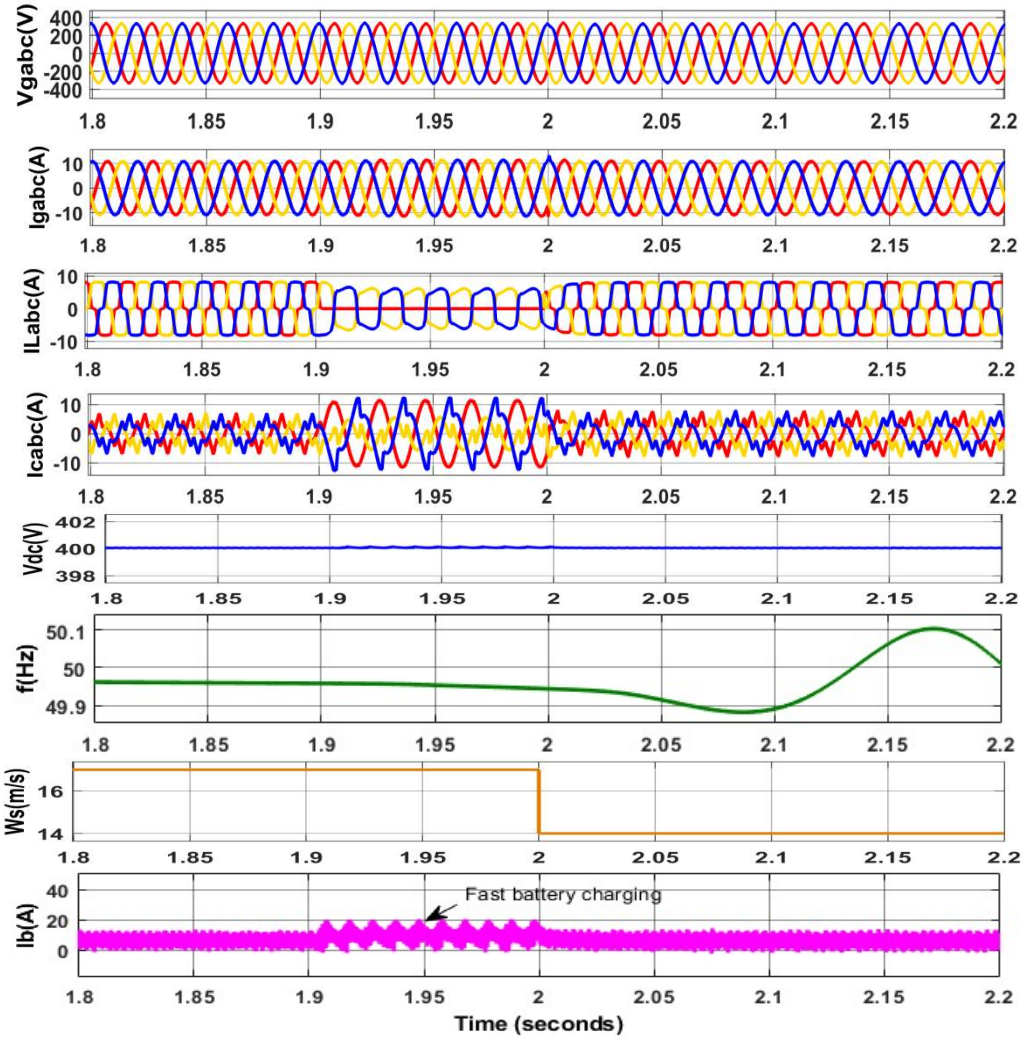

Figure.4 Performance under unbalanced loading and variable wind speed conditions

4.2 Performance under steady load and variable wind speed conditions

The performance of proposed system is also studied under the steady nonlinear conditions. The waveforms of source voltage (V_{gabc}), source current (I_{gabc}), three phase load current (I_{Labc}), compensator current (I_{Cabc}), dc link voltage, frequency at PCC and battery current (I_b) is observed and shown here in Figure.5 When the wind speed(Ws) is suddenly increased from 14m/s to 16m/s at t = 2.0 s. Resultantly wind power generation increases and extra power flowing towards BESS through VSC.Therefore, compensator current is slightly decreased, and battery charging current is increased . During increase in wind speed, BESS switches are in charging mode and maintain the balance of power at point of common coupling (PCC).

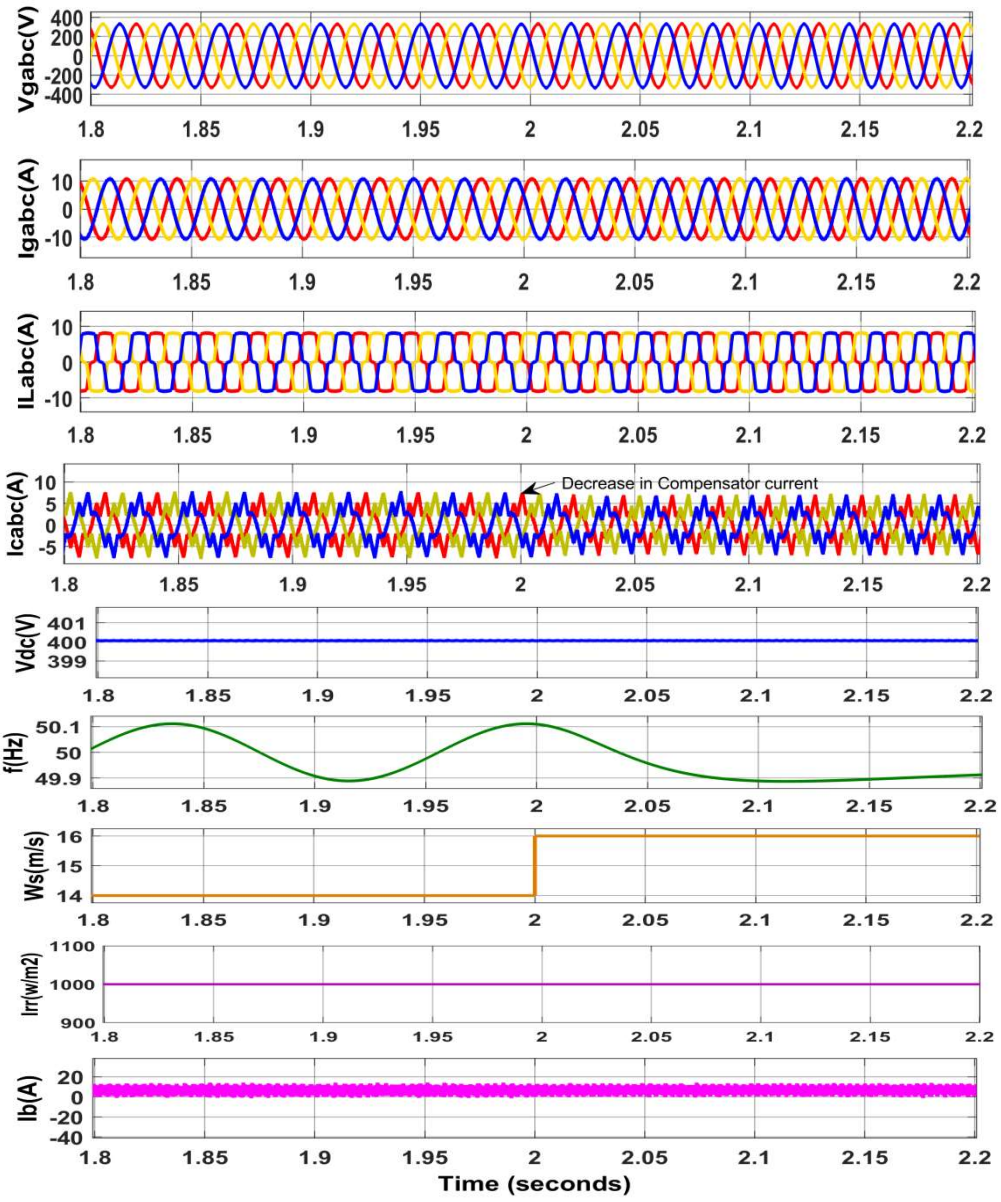

Figure.5 Performance under steady load and variable wind speed conditions

4.3 Performance under varying solar irradiance

The effective control action by adopted control is assessed under crucial operation of variable solar photovoltaic conditions and steady loading. The solar irradiance is changed from the level of 1000 w/m^2 to 650 w/m^2 with fixed wind speed feeding nonlinear load and its effects on dc voltage generation (V_{pv}), current generation (I_{pv}), power generation (P_{pv}) and duty cycle(D) of boost converter has been observed in Figure. 6(a).

The turbulence in the solar irradiation is generated at the instant of time t = 2.0 s. As a result, current and voltage generation from the solar panel is reduced upto certain extent. The duty cycle is also changed to operate the boost converter so that maximum power and stable dc voltage can be achieved. The waveforms of source voltage (V_{gabc}), source current (I_{gabc}), three phase load current (I_{Labc}), compensator current (I_{Cabc}), dc link voltage, frequency at PCC and battery current (I_b) is observed and shown here in

Figure.6 (b).

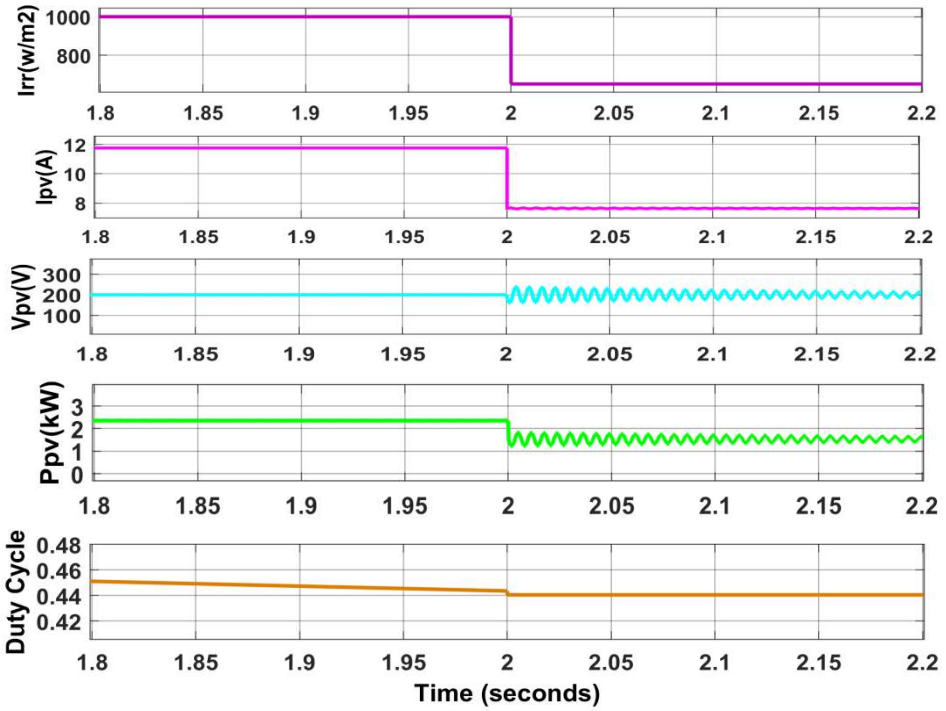
Irr(w/m2)
1000
800
Ipv(A)
12
10
8
Vpv(V)
300
200
100
Ppv(kW)
3
2
1
0
Duty Cycle
0.48
0.46
0.44
0.42
1.8 1.85 1.9 1.95 2 2.05 2.1 2.15 2.2
Time (seconds)

(a)

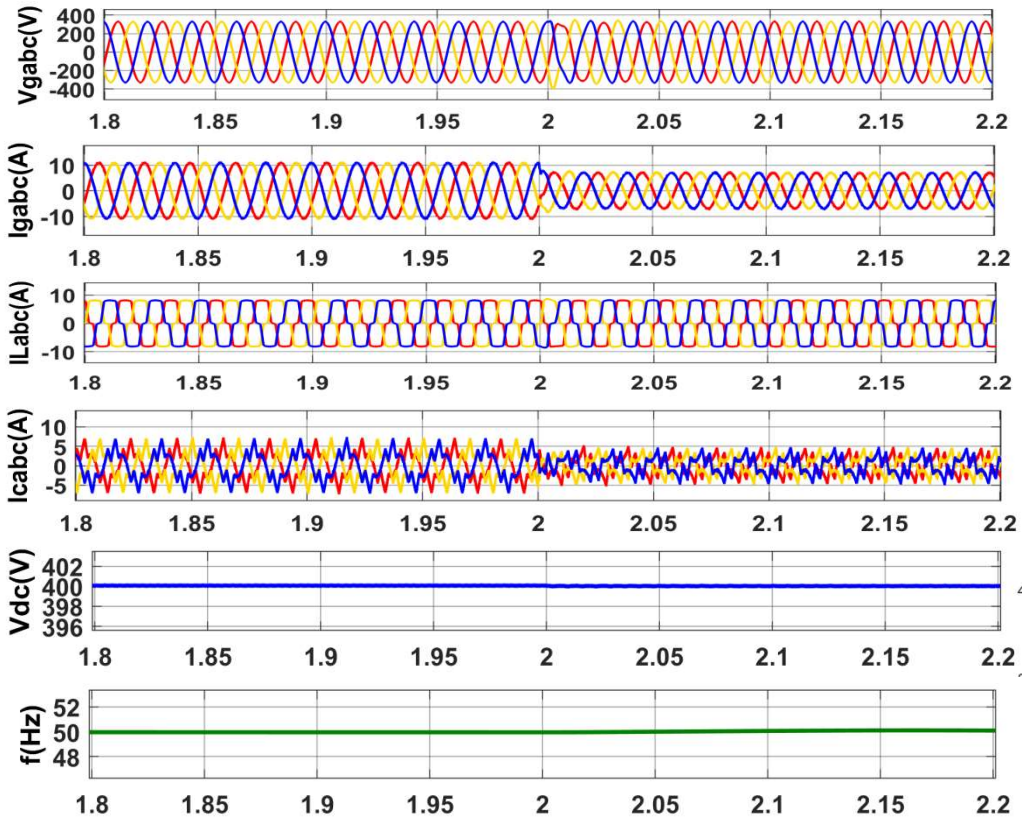
Vgabc(V)
400
200
0
-200
-400
Igabc(A)
10
0
-10
ILabc(A)
10
0
-10
Icabc(A)
10
5
0
-5
Vdc(V)
402
400
398
396
f(Hz)
52
50
48
1.8 1.85 1.9 1.95 2 2.05 2.1 2.15 2.2

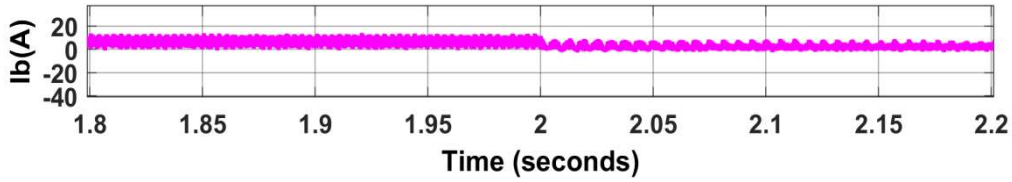

(b)

Figure.6 (a) and (b) Performance under varying solar irradiance

It is clear from the above waveforms that under variable solar irradiations the current from the supply affected in magnitude, however, its sinusoidal nature is not changed due to sinusoidal reference current. The source voltage is fully controlled in magnitude as well as in phase. It is also clear from the results that battery current is reversing its nature when power supply reduces from the less available solar irradiations. The dynamics in dc link and frequency curve is unnoticeable due to very effective control actions of applied control mechanism.

4.5 Harmonic Spectrum for Power Quality Assessment

The assessment of power quality of overall system taken for study was the major objective. Therefore, harmonic spectrum of source voltage, source current and load current is plotted and depicted in Figure.7 (a-c). From these plots, it can be observed that the total harmonic distortion (THD) in nonlinear load current is around 17% while THD level in source current and voltage is around 3.16 % and 1.01% respectively. This level of harmonics reduction in supply current and voltage is well accepted by IEEE-519 standard. Therefore, it is proved here that power quality in this supply system is always maintained as per pre specified limits.

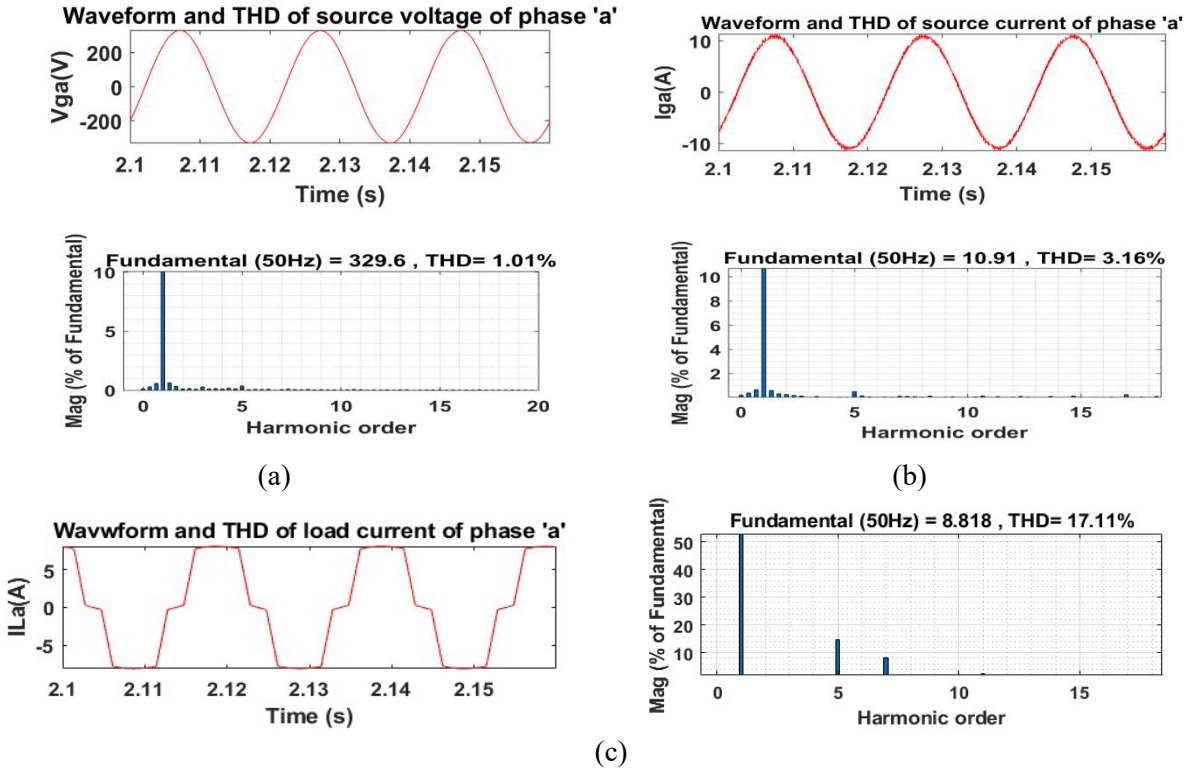

(a) (b)

(c)

Figure.7 Harmonic spectrum of standalone distributed generation system

4.6 Comparative study

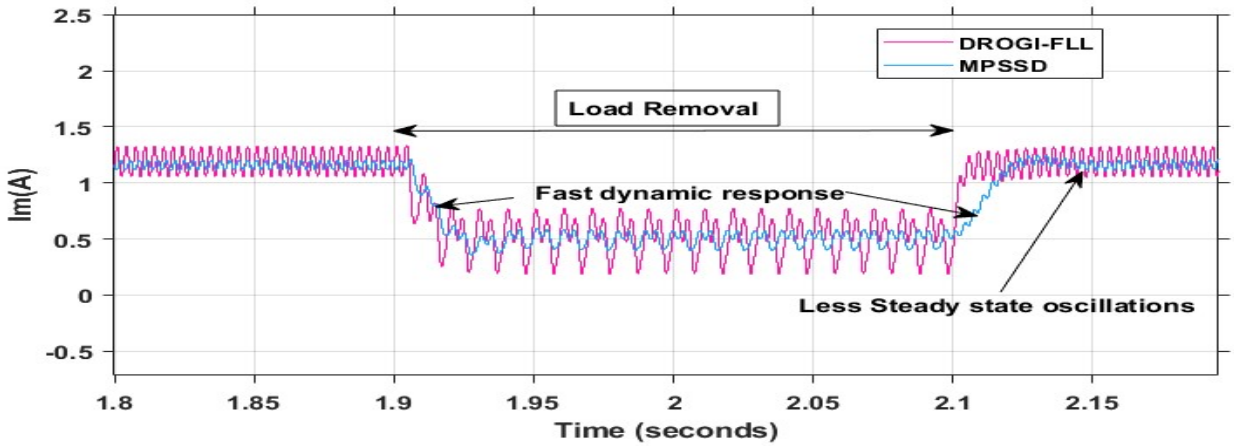

Figure.8 Comparative study

Figure.8 compares the performance of MPSSD and DROGI-FLL under a unbalanced load. The propose control has the best of fast dynamic response and less steady state oscillations under unbalanced load. The estimated amplitude (Im) of fundamental load current component is compared.

5. Conclusion

The objectives mentioned such as power quality, harmonic reduction, power factor correction and demand side management in the first section of this paper is successfully achieved using the modified parallel-structured signal decomposition algorithm (MPSSD). The effectiveness of this control algorithm is observed in the above simulation results with variable solar irradiations and wind speed. The entire system had been controlled and power quality standards are maintained. The system is operated in fully controlled mode and found satisfactory.

Appendix

Three-Phase SEIG:
Ratings: 3.7kW, 400V, 4-poles and 50Hz
Parameters: Rs = 1.405Ω,Ls = 0.0078H, Rr = 1.39 Ω ,Lr = 0.0078H,Inertia = 0.138,Friction = 0,pole pairs = 2,and Lf = 3Mh
PV System: Vpv = 252.32V,Ipv=11.69A
BESS parameters: 7.5Ah,400V,50% initial state of charge(SOC)
Non Linear Load: R =25 Ω,L = 300mH with three-phase diode rectifier
Control Parameters: PI controller-Kp=0.06,Ki = 0.007

References

[1] A. R. Jha, Wind Turbine Technology. London, U.K.: CRC Press, 2011.
[2] M. Godoy Simoes and F. A Farret, Alternate Energy Systems, Design and Analysis With Induction Generators, 2nd ed. London, U.K.: CRC Press, 2008.
[3] M. Stiebler, Wind Energy Systems for Electric Power Generation. Green Energy-1 and Technology, Berlin, Germany: Springer-Verlag, 2008.
[4] L. L. Lai andT. F. Chan, Distributed Generation: Induction and Permanent Magnet Generators. Hoboken, NJ, USA: Wiley, 2007.
[5] Bodson and S. C. Douglas, “Adaptive algorithms for the rejection of sinusoidal disturbances with unknown frequency,” Journal of Automatica, vol. 33, no. 12, pp. 2213-2221, Dec. 1997.

[6] D. Yazdani, M. Mojiri, A. Bakhshai, and G. Joos, "A fast and accurate synchronization technique for extraction of symmetrical components," IEEE Trans. on Power Electronics, vol. 24, no. 3, pp. 674-684, Mar. 2009.

[7] G. Yin, L. Guo, and X. Li, "An amplitude adaptive notch filter for grid signal processing," IEEE Trans. on Power Electronics, vol. 28, no. 6, pp. 2638-2641, Jun. 2013.

[8] A. B. Shitole, H. M. Suryawanshi, G. G. Talapur, S. Sathyan, M. S. Ballal, V. B. Borghate, M. R. Ramteke, and M. A. Chaudhari, "Grid interfaced distributed generation system with modified current control loop using adaptive synchronization technique," IEEE Trans. on Industrial Informatics, vol. 13, no. 5, pp. 2634-2644, Oct. 2017

[9] Y. Guan, J. C. Vasquez, J. M. Guerrero, Y. Wang and W. Feng, "Frequecy stability of hierarchically hybrid photovoltaic battery hydropower microgrids" IEEE trans. On industry applications, IEEE 2015

[10] S. Golestan, J. M. Guerrero, J. C. Vasquez, A. M. Abusorrah and T. Al-Turki, "A study on three phase FLLs" IEEE trans. On power electronics, IEEE 2018.

[11] Abhishek Kumar, SeemaKewat, Bhim Singh and Rashni Jain, "CC-ROGI-FLL based control for grid-tied photovoltaic system at abnormal grid conditions" IET generation, transmission and distribution, vol. 14, iss. 17, pp. 3400-3411, 2020

[12] Sanchit Mishra, I. Hussain, G. Pathak and Bhim Singh, "dPLL-based control of a hybrid wind-solar grid connected inverter in the distribution system" IET power electronics,vol. 11, iss. 5, pp. 952-960, 2018

[13] Saeed Golestan, J. M. Guerrero, and J. C. Vasquez, "Is using a complex control gain in three-phase FLLs reasonable" IEEE trans. On industrial electronics, vol. 67, no. 2, march 2020

[14] Ashutosh K. Giri, sabha Raj Arya, RakeshMaurya and B. ChittiBabu, "VCO-less PLL control-based voltage source converter for power quality improvement in distributed generation system" IET electric power applications, vol. 13, iss. 8, pp. 1114-1124, 2019

[15] X. Q. Guo and W. Y. Wu, "Simple synchronization technique for three phase grid-connected distributed generation systems," IET Renew. Power Gen., vol. 7, no. 1, pp. 55–62, Feb. 2013.

[16] X. Q. Guo, "Frequency-adaptive voltage sequence estimation for grid synchronization," Electronics Letters, vol. 46, no. 14, pp. 980–982, Jul. 2010.

[17] S. Vazquez, J. A. Snchez, M. R. Reyes, J. I. Leon, and J. M. Carrasco, "Adaptive vectorial filter for grid synchronization of power converters under unbalanced and/or distorted grid conditions," IEEE Trans. Ind. Electron., vol. 61, no. 3, pp. 1355–1367, Mar. 2014.

[18] Ashutosh K. Giri, Sabha Raj Arya and B. ChiitiBabu, "Power quality improvement in stand-alone SEIG-based distributed generation system using lorentzian norm adaptive filter" IEEE transactions on industry applications, Vol. 54, No. 5, Sept/oct 2018

[19] H. Wen, J. Zhang, Z. Meng, S. Guo, F. Li, and Y. Yang, "Harmonic Estimation Using Symmetrical Interpolation FFT Based on Triangular Self-Convolution Window," IEEE Transactions on Industrial Informatics, vol. 11, no. 1, pp. 16- 26, 2015.

[20] T. Tao, Z. Xinyan, and L. Bowen, "Analysis of harmonic and interharmonic detection based on Fourier-based synchrosqueezing transform and Hilbert transform," Power System Technology, vol. 43, no. 11, pp. 4200-4208, 2019.

[21] J. Roldán-Pérez, A. García-Cerrada, M. Ochoa-Giménez and J. L. Zamora- Macho, "Delayed-Signal-Cancellation-Based Sag Detector for a Dynamic Voltage Restorer in Distorted Grids," IEEE Trans. on Sust. Ener., vol. 10, no. 4, pp. 2015-2027, Oct. 2019.

[22] S. Golestan, F. D. Freijedo, A. Vidal, A. G. Yepes, J. M. Guerrero and J. Doval-Gandoy, "An Efficient Implementation of Generalized Delayed Signal Cancellation PLL," IEEE Trans. Power Electron., vol. 31, no. 2, pp. 1085-1094, Feb. 2016.

[23] Wang, SY, Etemadi, A and Doroslovacki, M. Adaptive cascaded delayed signal cancellation PLL for three-phase grid under unbalanced and distorted condition[J]. Electr. Pow. Syst. Res., 2020, 180:106165.

[24] Zheng Wu, Chenwen Cheng, Wei Hua, Yuchen Wang, Hengliang Zhang, Wei Wang, "A Frequency-Adaptive Delay Signal Cancelation Based Filter to Reduce Position Estimation Error for Sensorless IPMSM Drives", IEEE Trans. Power Electron., vol.38, no.2, pp.1662-1671, 2023.

[25] Ashutosh K. Giri, Sabha Raj Arya and RakeshMaurya, "Compensation in power quality problems in wind based renewable energy system for small consumer as isolated loads" IEEE trans. On industrial electronics, vol. 66, no. 11, november 2019

[26] S. Gude and C. -C. Chu, "Three-Phase PLLs by Using Frequency Adaptive Multiple Delayed Signal Cancellation Prefilters Under Adverse Grid Conditions," IEEE Trans. Ind. Appl., vol. 54, no. 4, pp. 3832-3844, July- Aug. 2018.

[27] Saeed Golestan, Josep M. Guerrero, Juan C. Vasquez,Abdullah M. Abusorrah, and Yusuf Al-Turki, "Harmonic Linearization and Investigation of Three-Phase Parallel-Structured Signal Decomposition Algorithms in Grid-Connected Applications" Accepted in " IEEE trans. On industrial electronics, DOI 10.1109/TPEL.2020.3021723, 2023.

[28] Jaklair, Lingappa, Guduri Yesuratnam, and Pannala Mallikarjuna Sarma. "Control Algorithm for Renewable Energy Standalone System with Power Quality and Demand Management." *Majlesi Journal of Electrical Engineering* (2024).